Deexcitation of dipole emitters in finite ordered charge-sheet structures

Agus Muhamad Hatta,[1,2,*] Ali A. Kamli,[1] and M. Babiker[3]

[1]*Department of Physics, Faculty of Science, Jazan University, P.O. Box 114, Jazan, Saudi Arabia*
[2]*Department of Engineering Physics, Institut Teknologi Sepuluh Nopember, Surabaya, Indonesia*
[3]*Department of Physics, University of York, Heslington, York YO10 5DD, United Kingdom*

Layered structures consisting of finite numbers of charge sheets separating dielectric layers are considered as physically realizable media for the control of dipole deexcitation due to spontaneous emission. The dispersion relation and the corresponding field distributions of a general structure are determined using transfer-matrix techniques. An excited dipole emitter localized in the vicinity of the truncation layer is coupled to the fields supported by such a structure, and its deexcitation rate is evaluated for a number of scenarios in which the structure is characterized by different numbers of charge sheets for varying excitation frequency and varying emitter position. The analysis highlights significant enhancements of the deexcitation rate which can be readily controlled through the adjustable parameters of the structure.

I. INTRODUCTION

It is well known that the rate of deexcitation of a dipole emitter in the form of an atom, a molecule, or a quantum dot can be controlled by modifying the electromagnetic environment in which the emitter, regarded as a quantum bit (qubit), is localized. One of the striking features of a controlled environment occurs when the emitter is localized within a periodic structure. The periodicity leads to the appearance of band gaps in the frequency spectrum, and such band gaps arise when the wavelength is comparable to the superlattice period. If the excitation frequency lies within one of the frequency band gaps of the structure, the emitter cannot release its excitation energy, as it would in the unbounded bulk, and so its lifetime is greatly enhanced [1–4]. For excitation frequencies lying near a band edge it has been pointed out that the enhanced density of states leads to enhanced deexcitation [5,6]. The possibility of tailoring the electromagnetic environment for specific outcomes using layered systems is significant, with implications for useful applications in which the emitters serve as elements in quantum circuits and quantum memory. Other recognized applications involve use in low-threshold lasers and other low-power consumption photonic devices [7].

The periodic structure consists of a set of dielectric sheets periodically separating a set of layers of a different dielectric. There have been considerable advances in the micro- and nanofabrication of layered structures such as mentioned above using deposition and lithographic techniques and exploiting the clear flexibility afforded by the variety of material combinations forming the dielectric and charge sheets. The charge sheet can be formed as a two-dimensional electron gas trapped in an inversion layer or in a quantum well achieved by modulation doping [8,9]. It is known that the characteristic frequencies of the charge-sheet-structure systems fall within the terahertz (THz) or infrared wavelength range, and it is beneficial for the development of compact devices operating within this frequency range [10].

Meanwhile, the layered structure of the dielectric and charged sheets in superlattice forms has been shown to exhibit many interesting physical properties. In the past few decades, the properties of collective excitations in infinite and semi-infinite superlattices have been studied intensively [11–15]. The characteristics of bulk plasmons and surface plasmon modes in various structures have also been explored, including infinite and semi-infinite charge-sheet superlattices [15]. The periodicity of an infinite superlattice permits the application of Bloch's theorem, which leads to considerable simplifications of the analysis. In the truncated charge-sheet system at hand, the translational symmetry is not preserved, Bloch's theorem may not be appropriate, and we use the transfer-matrix exact calculations here. As far as we are aware, previous treatments did not proceed to determine the influence of superlattice modes on emitters localized within the structure and in the vicinity of the surface. More recent work on plasmonic superlattices considered the interesting issues of the influence of defects in the superlattice periodicity on the frequency spectra [16].

In this paper the charge-sheet dielectric structures are considered with special emphasis on the case of a finite number of layers, and the analysis is carried out using transfer-matrix methods. The objective is not only to determine the dispersion relation and the quantized fields of the structure but also to evaluate the coupling of the fields to excited dipole emitters. The rate of the deexcitation of an emitter localized within the structure and near the truncation surface is evaluated as well as the variations of the deexcitation rate with the adjustable parameters of the system, including the emitter position, the excitation frequency, and the number of charge sheets in the layered structure.

II. THE ELECTROMAGNETIC ENVIRONMENT

The charge-sheet dielectric system under consideration is shown in Fig. 1. The region of space $z < 0$, hitherto referred to as the surface or capping layer, is occupied by a homogeneous dielectric of dielectric constant ϵ_s. The plane $z = 0$ is occupied by a charge sheet (labeled $l = 1$) deposited on the first dielectric layer (labeled $n = 0$). The space $0 <$

_____
*ahatta@jazanu.edu.sa
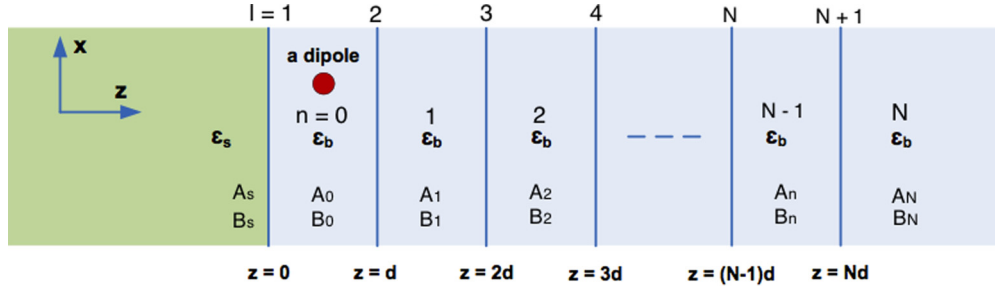
FIG. 1. (Color online) Schematic representation of the finite charge-sheet dielectric structure. See the text for the description of the layer labels and the parameters.

$z < Nd$ is occupied by N dielectric layers of equal thickness d and dielectric constant ϵ_b, and these dielectric layers are separated by the charge sheets occupying the planes $z = nd$ ($n = 0,1,2,\ldots,N$). Finally, the region of space $z > Nd$ is occupied by a substrate layer with a dielectric constant ϵ_b.

The electric-field vector $\mathbf{E}$ of a transverse mode of frequency ω satisfies the wave equation

$$\nabla^2 \mathbf{E} + \left(\frac{\epsilon_i \omega^2}{c^2}\right)\mathbf{E} = 0, \tag{1}$$

where $\epsilon_i = \epsilon_s, \epsilon_b$ are the dielectric constants of the capping layer and substrate layer, respectively, and c is the velocity of light in vacuum. The solution of the interface-type modes in any layer can be written as

$$\mathbf{E}(\mathbf{r},t) = \begin{cases} B_s\left[\left(\hat{\mathbf{r}}_\parallel - \frac{i\mathbf{k}_\parallel}{\beta_s}\hat{z}\right)e^{\beta_s z}\right]e^{i(\mathbf{k}_\parallel \cdot \mathbf{r} - \omega t)}, & z < 0; \\ \left\{A_n\left[\left(\hat{\mathbf{r}}_\parallel + \frac{i\mathbf{k}_\parallel}{\beta}\hat{z}\right)e^{\beta(z-nd)}\right] + B_n\left[\left(\hat{\mathbf{r}}_\parallel - \frac{i\mathbf{k}_\parallel}{\beta}\hat{z}\right)e^{-\beta(z-nd)}\right]\right\}e^{i(\mathbf{k}_\parallel \cdot \mathbf{r} - \omega t)}, & 0 < z < nd; \\ A_N\left[\left(\hat{\mathbf{r}}_\parallel + \frac{i\mathbf{k}_\parallel}{\beta}\hat{z}\right)e^{-\beta(z-Nd)}\right]e^{i(\mathbf{k}_\parallel \cdot \mathbf{r} - \omega t)}, & z > Nd; \end{cases} \tag{2}$$

where $A_{n,N}$ and $B_{s,n}$ are the field amplitudes, $\beta_s = (k_\parallel^2 - \frac{\epsilon_s \omega^2}{c^2})^{1/2}$ and $\beta = (k_\parallel^2 - \frac{\epsilon_b \omega^2}{c^2})^{1/2}$ are the wave numbers in the surface layer and the n layer, and $k_\parallel$ is the wave number parallel to the interfaces. It should be noted that the amplitudes B_N and A_s are zeros because it is assumed no waves can enter from the right side of the Nth layer or from the left side in the capping layer. Using Maxwell's equation $\mathbf{H} = \frac{\epsilon_0 c^2}{i\omega}\nabla \times \mathbf{E}$, the corresponding magnetic fields can be readily determined.

The presence of the two-dimensional charge sheets at interfaces presents jump conditions on the tangential component of the magnetic field [17] in addition to the continuity of the tangential component of the electric field. Applying the continuity of the tangential $\mathbf{E}$ at the interface $z = 0$, between the capping layer and the first dielectric layer $n = 0$, we have

$$E_x^{(s)} = E_x^{(0)}. \tag{3}$$

From Eq. (3), the field-amplitude relation can be written as

$$B_s = A_0 + B_0. \tag{4}$$

The second boundary condition on the continuity of the tangential component of $\mathbf{H}$ can be written in terms of the electric field using one of Maxwell's equations at $z = 0$ as

$$\hat{z} \times (\nabla \times \mathbf{E}^{(0)} - \nabla \times \mathbf{E}^{(s)}) = \sigma E_x^{(0)}, \tag{5}$$

where σ is the two-dimensional conductivity defined by

$$\sigma = \frac{i n_s e^2}{m^*(\omega + i\gamma)}, \tag{6}$$

with n_s being the areal electron density, e and m^* being the electron charge and effective mass, and the damping rate $\gamma \ll \omega$. From Eq. (5) we obtain

$$\frac{\epsilon_0 \epsilon_b \omega}{i\beta}[A_0 - B_0] + \frac{\epsilon_0 \epsilon_s \omega}{i\beta_s}B_s = -\sigma[A_0 + B_0]. \tag{7}$$

From Eqs. (4) and (7), the amplitudes A_0 and B_0 can be expressed via a transfer matrix as

$$\begin{bmatrix} A_0 \\ B_0 \end{bmatrix} = \mathbf{T_s}\begin{bmatrix} 0 \\ B_s \end{bmatrix}, \tag{8}$$

where

$$\mathbf{T_s} = \frac{1}{2}\begin{bmatrix} 0 & \left(1 + \frac{\Omega^2 \beta d}{\omega^2} - r_s\frac{\beta}{\beta_s}\right) \\ 0 & \left(1 - \frac{\Omega^2 \beta d}{\omega^2} + r_s\frac{\beta}{\beta_s}\right) \end{bmatrix}, \tag{9}$$

with $r_s = \frac{\epsilon_s}{\epsilon_b}$ being the permittivity ratio and Ω being a scaling frequency defined by

$$\Omega^2 = \frac{n_s e^2}{m^* \epsilon_0 \epsilon_b d}. \tag{10}$$

Similarly, at successive layer surfaces $z = d, 2d, \ldots, Nd$, repeated application of the boundary condition tangential $\mathbf{E}$ continuous leads to the determination of the amplitudes A_n and B_n, which can be expressed via a transfer matrix as follows:

$$\begin{bmatrix} A_1 \\ B_1 \end{bmatrix} = \mathbf{T}\begin{bmatrix} A_0 \\ B_0 \end{bmatrix}, \tag{11}$$

where

$$\mathbf{T} = \frac{1}{2}\begin{bmatrix} m_{11} & m_{12} \\ m_{21} & m_{22} \end{bmatrix}, \tag{12}$$

with

$$m_{11} = (2 + \eta)e^{-\beta d}, \tag{13a}$$

$$m_{12} = \eta e^{\beta d}, \tag{13b}$$

$$m_{21} = -\eta e^{-\beta d}, \tag{13c}$$

$$m_{22} = (2 - \eta)e^{\beta d}, \tag{13d}$$

where $\eta = \frac{\Omega^2 \beta d}{\omega^2}$. Thus the field amplitudes in the whole structure comprising N layers can be expressed in matrix form using Eqs. (8) and (11). We have for an N-layer system

$$\begin{bmatrix} A_N \\ 0 \end{bmatrix} = \mathbf{T^n T_s} \begin{bmatrix} 0 \\ B_s \end{bmatrix}, \tag{14}$$

where $\mathbf{T^n} = \mathbf{XD^n X^{-1}}$, with $\mathbf{X}$ being an eigenvector matrix of $\mathbf{T}$ and $\mathbf{D}$ being a diagonalized eigenvalue matrix of $\mathbf{T}$. The above analysis provides the basis for the evaluation of the dispersion relation in the following.

III. DISPERSION RELATION

The dispersion relation for this structure can be evaluated numerically by solving the matrix component of $(\mathbf{T^n T}_s)_{22} = 0$. In the case $r_s = 1$, it is known that $\mathbf{T}_s = \mathbf{T^n}$; then the matrix element $(\mathbf{T^n T}_s)_{22}$ becomes $(\mathbf{T}^{n+1})_{22}$, and after some algebra, it can be written in the form

$$(\mathbf{T}^{n+1})_{22} = \frac{1}{2C}[(M_1 + C)(M_2 - C)^{n+1}$$
$$- (M_1 - C)(M_2 + C)^{n+1}], \tag{15}$$

where $M_1 = \frac{1}{2}(m_{11} - m_{22})$, $M_2 = \frac{1}{2}(m_{11} + m_{22})$, and $C^2 = M_2^2 - m_{11}m_{22} + m_{12}m_{21}$.

In a layer system for which the dielectric constants satisfy $r_s \neq 1$, the matrix elements of $(\mathbf{T^n T}_s)_{22}$ emerge in the form

$$(\mathbf{T^n T}_s)_{22} = \frac{1}{4m_{12}C}\Big\{\big[(M_1^2 - C^2)\lambda_1^n + (M_1 - C)$$
$$\times (-M_1 - C)\lambda_2^n\big]D_1 + \big[m_{12}(M_1 + C)\lambda_1^n$$
$$- m_{12}(M_1 - C)\lambda_2^n\big]D_2\Big\}, \tag{16}$$

where $\lambda_{1,2} = M_2 \mp C$ and $D_{1,2} = 1 \pm \eta \mp r_s \frac{\beta}{\beta_s}$.

Figure 2 shows the dispersion curves arising from Eq. (15) for the case of $r_s = 1$ and for different layer numbers N. The parameters used for calculations are as follows: $\epsilon_b = 12.90$, $n_s = 6 \times 10^{15}$ m^{-2}, $d = 100$ nm, $e = 1.60 \times 10^{-19}$ C, $m^* = 9.11 \times 10^{-31}$ kg. Figures 2(a)–2(d) present the dispersion relations of the finite charge-sheet dielectric structures with layer numbers given by $N = 0$, $N = 1$, $N = 5$, and $N = 50$, respectively. For $N = 0$ as in Fig. 2(a), only one mode of the interface type exists, which was described earlier by Albuquerque and Cottam [14]. The interface-type dispersion
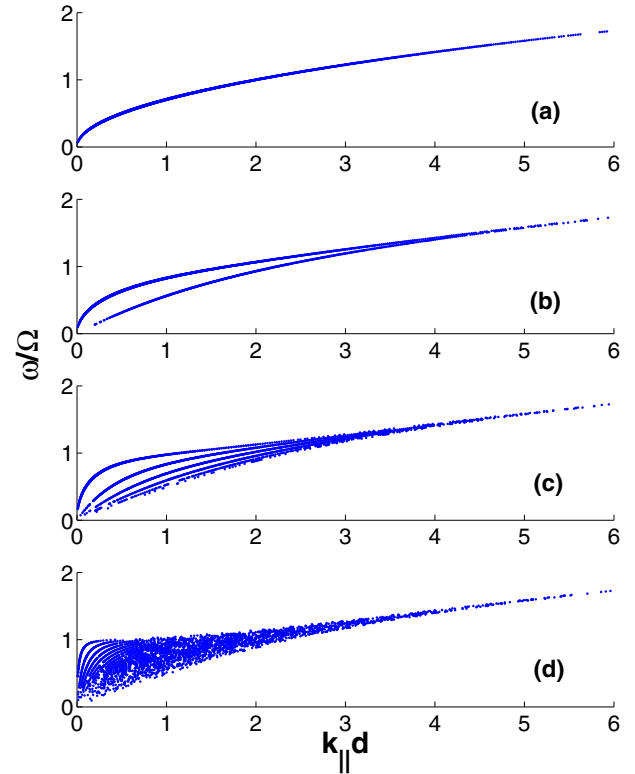
FIG. 2. (Color online) Dispersion relation for the case of $r_s = 1$ with the number of finite layers (a) $N = 0$, (b) $N = 1$, (c) $N = 5$, and (d) $N = 50$.

relation in the form of $\omega = [\Omega c k_\parallel/(\epsilon_s + \epsilon_b)]^{1/2}$ [14] for $N = 0$ is in agreement with the calculation presented in this paper.

The case $N = 1$ is shown in Fig. 2(b); there are two modes, both of which can be described as interface type, and this conforms with what is expected since the structure has two charge sheets. It is also found that for $N = 5$ (six charge sheets) there are six modes of the interface type, as in Fig. 2(c). When the number of layers is sufficiently large [$N = 50$; see Fig. 2(d)], the dispersion relation becomes similar to the so-called bulk mode in the case of an infinite charge-sheet superlattice structure [15]. For comparison, we display the case of the bulk-mode-dispersion relation of the infinite charge-sheet system using the well-known dispersion relation $\frac{\omega}{\Omega} = \big[\frac{k_\parallel d \sinh(k_\parallel d)}{2[\cosh(k_\parallel d) - \cos(Qd)]}\big]^{1/2}$ in [14], as is shown in Fig. 3 (shaded region).

Figure 3 presents the interface-type dispersion relation for the case of $r_s \neq 1$ and $N = 5$ using Eq. (16) for different $r_s = 0.1, 0.5, 0.9, 1.1, 2$, and 10. It can be seen that for each value of r_s, there is only one mode, as is well known for surface modes [15]. It is also found that the surface-mode branch emerges out of the bulk modes higher in frequency for the case $r_s < 1$ and lower in frequency for the case $r_s > 1$. The surface modes have previously been identified as satisfying the equation $[r_s \sinh(k_\parallel d) + \cosh(k_\parallel d)]k_\parallel d(\frac{\Omega}{\omega})^2 + (r_s^2 - 1)\sinh(k_\parallel d) = 0$ [15]. The results in this paper are seen to be in agreement with this analytical result.
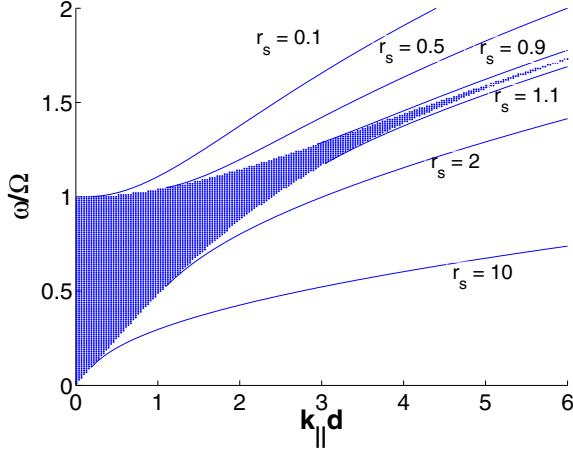
FIG. 3. (Color online) Bulk dispersion relation calculated using a well-known expression in [15] (shaded region) and interface-type mode dispersion curves for several variations of r_s calculated using Eq. (16).

IV. FIELD PROFILES

The field profiles of the interface-type modes are plotted using Eq. (2). Once the wave number $k_\parallel$ or the frequency ω is obtained using (15) or (16), the remaining task is to calculate the field amplitudes in any layer n. Consider the transfer matrix again in the form

$$\begin{bmatrix} A_n \\ B_n \end{bmatrix} = \mathbf{T^n T_s} \begin{bmatrix} 0 \\ B_s \end{bmatrix}. \qquad (17)$$

The field amplitudes within layer n, namely, A_n and B_n, can be calculated from the matrix elements of $\mathbf{T^n T_s}$. It is found that $(\mathbf{T^n T_s})_{11} = (\mathbf{T^n T_s})_{21} = 0$, and $(\mathbf{T^n T_s})_{22}$ is already given by Eq. (16). The matrix elements $(\mathbf{T^n T_s})_{12}$ can be written as

$$(\mathbf{T^n T_s})_{12} = \frac{1}{4m_{12}C} \Big\{ \big[-m_{12}\lambda_1^n(M_1 - C) - m_{12}\lambda_2^n \\ \times (-M_1 - C) \big] D_1 + \big[m_{12}^2 \lambda_2^n - m_{12}^2 \lambda_1^n \big] D_2 \Big\}, \qquad (18)$$

where we have set $\lambda = \lambda_1 = \frac{1}{\lambda_2} = e^\alpha$. After some algebra the field amplitudes emerge in the form

$$A_n = \frac{1}{2\sinh\alpha} \left\{ \left[\sinh(n-1)\alpha - \left(1 + \frac{\eta}{2}\right) e^{-\beta d} \sinh n\alpha \right] \right. \\ \left. \times D_1 - \left[\frac{\eta}{2} e^{\beta d} \sinh n\alpha \right] \times D_2 \right\} B_s, \qquad (19a)$$

$$B_n = \frac{1}{2\sinh\alpha} \left\{ \left[\frac{\eta}{2} e^{-\beta d} \sinh n\alpha \right] \times D_1 \right. \\ \left. + \left[\sinh(n-1)\alpha - \left(1 - \frac{\eta}{2}\right) e^{\beta d} \sinh n\alpha \right] \times D_2 \right\} B_s, \qquad (19b)$$
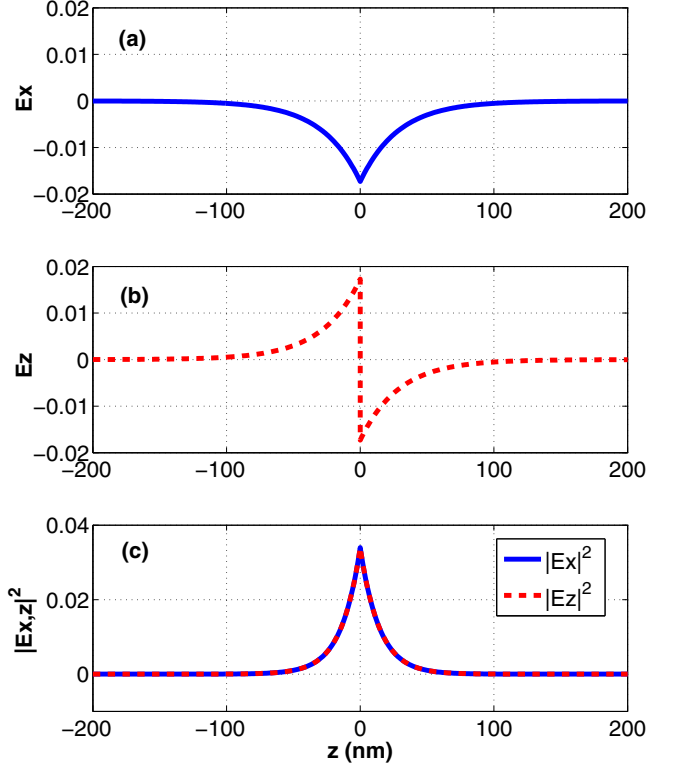
FIG. 4. (Color online) Distribution of the electric field and its intensity for a single charge sheet between two slabs, the capping layer and the substrate; (a) E_x (b) E_z, and (c) the intensity profile $|E_{x,z}|^2$ for $N = 0$, $k_\parallel d = 3.5$ and $r_s = 1$.

$$A_N = \frac{1}{2\sinh\alpha} \left\{ \left[\sinh(N-1)\alpha - \left(1 + \frac{\eta}{2}\right) e^{-\beta d} \sinh N\alpha \right] \right. \\ \left. \times D_1 - \left[\frac{\eta}{2} e^{\beta d} \sinh N\alpha \right] \times D_2 \right\} B_s. \qquad (19c)$$

Figures 4–7 display the normalized field and intensity profiles (in arbitrary units). Figure 4 shows the field profiles for the case of $N = 0$, $k_\parallel d = 3.5$, and $r_s = 1$. Figures 4(a)–4(c) display the tangential component E_x, the normal component E_z, and intensities $|E_{x,z}|^2$ for the mode featured in Fig. 2(a). It is seen that the field distributions are localized at the interface. The continuity of E_x and the discontinuity of E_z at the interface are evident. This feature has also been addressed in [16]. It is also seen from the intensity profiles in Figure 4(c) that both the tangential and normal components have similar distributions.

Figure 5 shows the field profiles for the case $N = 1$, $k_\parallel d = 3.5$, and $r_s = 1$. The corresponding dispersion relation in this case is depicted in Fig. 2(b), involving two modes. Figures 5(a)–5(c) correspond to the tangential component E_x, the normal component E_z, and their intensities $|E_{x,z}|^2$ for the first mode, while Figs. 5(d)–5(f) correspond to fields and intensities for the second mode. It can be seen that the first and second modes both possess one symmetric and one antisymmetric field distribution, as shown in Figs. 5(a) and 5(d) and 5(b) and 5(e). The intensity distributions have similar shapes but differ in the magnitudes of the intensity.
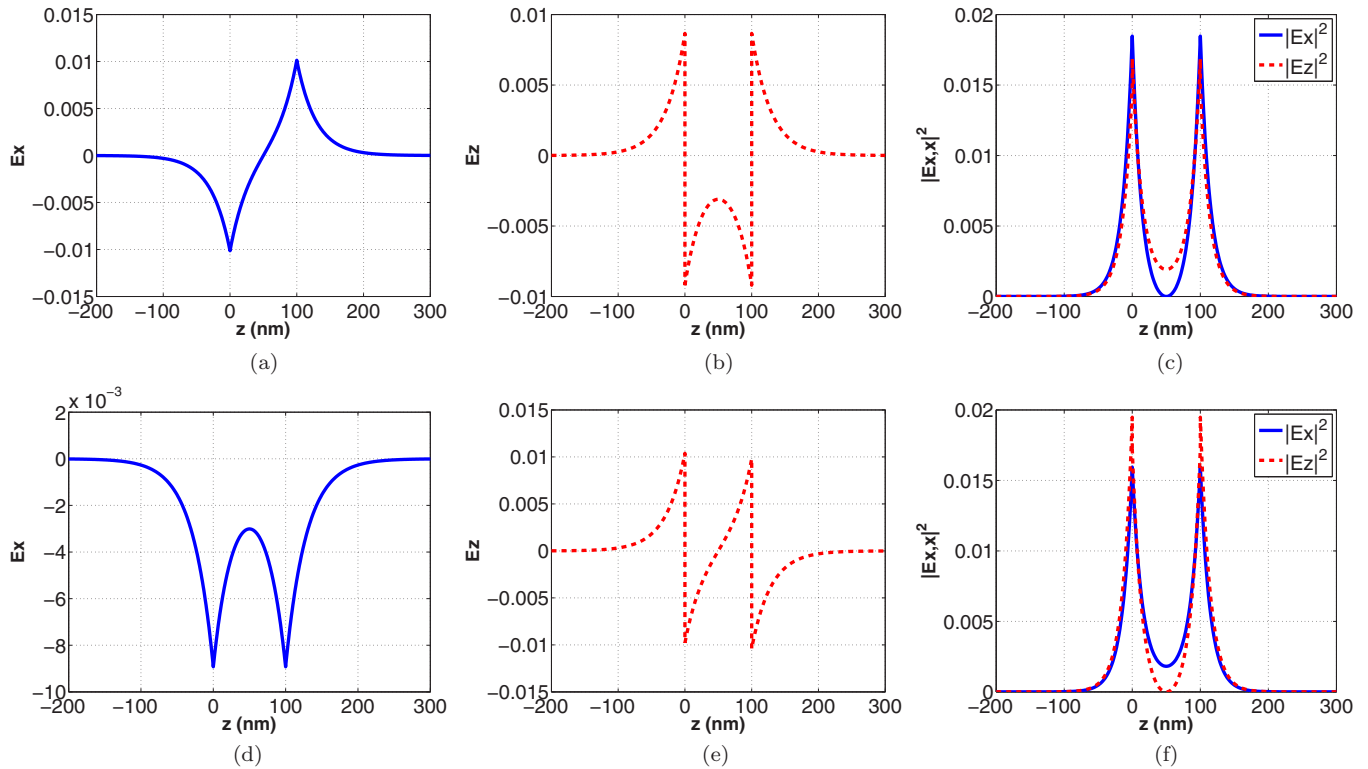
FIG. 5. (Color online) Field profile of the electric field and its intensity for the two-charge-sheet structure in which there are two modes (for the case $N = 1$, $k_\parallel d = 3.5$, and $r_s = 1$): shown are (a) E_x, (b) E_z, and (c) $|E_{x,z}|^2$ for mode 1 and (d) E_x, (e) E_z, and (f) $|E_{x,z}|^2$ for mode 2.

Figure 6 shows the intensity profiles for the case of $N = 5$, $k_\parallel d = 3.5$, with several r_s values. Figures 6(a)–6(c)
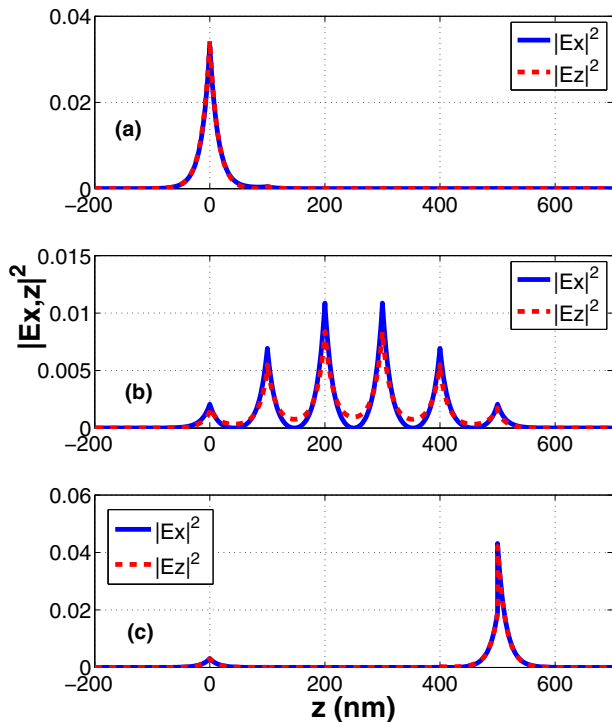
FIG. 6. (Color online) The intensity with the variation of r_s for $N = 5$ and $k_\parallel d = 3.5$ at (a) $r_s = 0.5$, (b), $r_s = 1$, and (c) $r_s = 2$.

correspond to the cases $r_s = 0.5$, $r_s = 1$, $r_s = 2$, respectively. The dispersion relation corresponding to Fig. 6(a) is shown in Fig. 3. In Fig. 6(a), it is seen that the intensities are localized at the first interface. The dispersion relation corresponding to Fig. 6(b) is shown in Fig. 2(c). It is clear that the intensities are localized at each interface but are concentrated in the middle layers. The dispersion relation corresponding to Fig. 6(c) is displayed in Fig. 3. Two localized intensities can be seen at the beginning and end layers, with a higher intensity at the end layer. From Fig. 6, it is clear that the intensity profile strongly depends on r_s. In the case $r_s = 1$, the intensity profile leads to the known profile of a bulk plasmon mode, and for $r_s \neq 1$, the intensity profile has surface-mode features.

Figure 7 explores the effect of the variation in the normalized wave number $k_\parallel d$ on the intensity profile for the case of $N = 5$. Figures 7(a)–7(c) show the intensity profiles in the case of $r_s = 0.9$ for $k_\parallel d = 2$, 4.6, and 6, respectively. In Fig. 7(a), it is seen that the intensity profile has the bulk-mode character, as the wave number of $k_\parallel d = 2$ is below the cutoff wave number for the surface mode. The cutoff wave number corresponds to $k_\parallel d = \ln |(1 + r_s)/(1 - r_s)|$ [15], which equals 2.944. It is also shown that the profile has an asymmetric shape compared to the case of $r_s = 1$, which is symmetric, as in Fig. 6(b). Figure 7(b) shows the intensity profile of the surface modes. Above the cutoff wave number, the intensity is localized at the first interface and has low intensity at the second interface, as shown in Fig. 7(b). However, for a higher normalized wave number, $k_\parallel d = 6$, the intensity is peaked at the end interface and very low at the first interface, as shown in Fig. 7(c). The characteristics of the field and intensity profiles due to
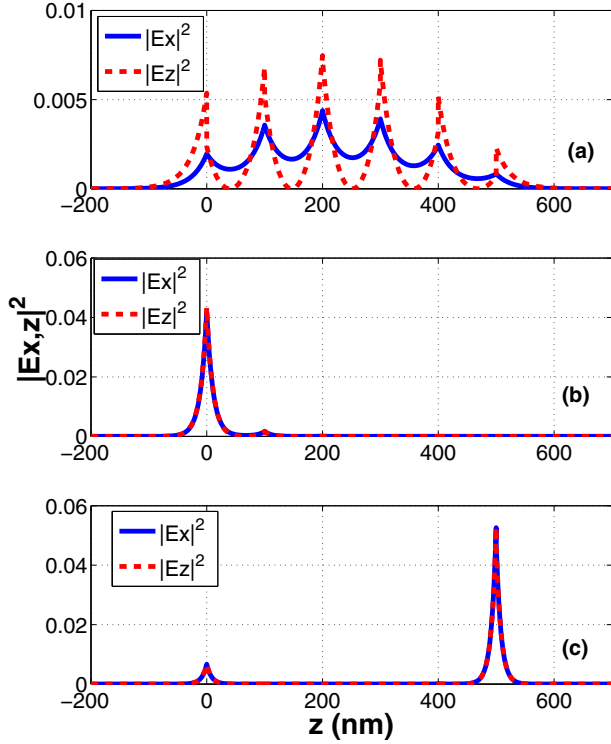
FIG. 7. (Color online) The intensity distribution for $N = 5$ and $r_s = 0.9$, with a normalized wave number (a) $k_\parallel d = 2$, (b) $k_\parallel d = 4.6$, and (c) $k_\parallel d = 6$.

the structure parameters and wave numbers are important in studying the deexcitation rate since the dipole emitter embedded in the layer is coupled to the electric-field operator, as will be shown. In the next sections, the field quantization and the evaluation of the deexcitation rate are considered.

V. FIELD QUANTIZATION

To quantize the electromagnetic field of the structure, we follow the procedure given in [5,17]. The electromagnetic field Hamiltonian is given by

$$H_{\text{field}} = \frac{1}{2}\epsilon_0 \int [\epsilon_i |\hat{\mathbf{E}}|^2 + c^2 |\hat{\mathbf{B}}|^2] d^3\mathbf{r}, \qquad (20)$$

where $\epsilon_i = \epsilon_s$ or ϵ_b. The electric-field operator $\hat{\mathbf{E}}$ is written in quantized form as

$$\hat{\mathbf{E}}(\mathbf{r},t) = \int d^2\mathbf{k}_\parallel C_0(\mathbf{k}_\parallel)[\mathbf{E}(\mathbf{r}_\parallel,z,\mathbf{k}_\parallel)a(\mathbf{k}_\parallel) + \text{H.c.}], \quad (21)$$

where $a(\mathbf{k}_\parallel)$ and $a^\dagger(\mathbf{k}_\parallel)$ are boson operators satisfying the commutation relation

$$[a(\mathbf{k}_\parallel),a^\dagger(\mathbf{k}'_\parallel)] = \delta(\mathbf{k}_\parallel - \mathbf{k}'_\parallel). \qquad (22)$$

The electric-field vector $\mathbf{E}(\mathbf{r}_\parallel,z,\mathbf{k}_\parallel)$ is defined in the different regions as follows. In the region $z < 0$,

$$\mathbf{E}^{(s)} = C_0(\mathbf{k}_\parallel) B_s \left(\hat{\mathbf{r}}_\parallel - i\frac{k_\parallel}{\beta_s}\hat{z}\right) e^{\beta_s z} e^{i(\mathbf{k}_\parallel \cdot \mathbf{r} - \omega t)}. \qquad (23)$$

Within layer n, the expression for the electric-field vector is

$$\mathbf{E}^{(n)} = C_0(\mathbf{k}_\parallel)(\hat{\mathbf{r}}_\parallel F^{(n)} + \hat{z} G^{(n)}) e^{i(\mathbf{k}_\parallel \cdot \mathbf{r} - \omega t)}, \qquad (24)$$

where

$$F^{(n)} = A_n e^{\beta(z-nd)} + B_n e^{-\beta(z-nd)}, \qquad (25)$$

$$G^{(n)} = \frac{ik_\parallel}{\beta}(A_n e^{\beta(z-nd)} - B_n e^{-\beta(z-nd)}). \qquad (26)$$

Finally, in the region $z > Nd$, the electric-field vector is

$$\mathbf{E}^{(N)} = C_0(\mathbf{k}_\parallel) A_N(\mathbf{k}_\parallel)\left(\hat{\mathbf{r}}_\parallel + i\frac{k_\parallel}{\beta}\hat{z}\right) e^{\beta z} e^{i(\mathbf{k}_\parallel \cdot \mathbf{r} - \omega t)}. \quad (27)$$

$C_0(\mathbf{k}_\parallel)$ is an overall factor such that the field Hamiltonian reduces to the canonical form

$$H_{\text{field}} = \frac{1}{2}\int d^2\mathbf{k}_\parallel \hbar\omega(\mathbf{k}_\parallel)[a(\mathbf{k}_\parallel)a^\dagger(\mathbf{k}_\parallel) + a^\dagger(\mathbf{k}_\parallel)a(\mathbf{k}_\parallel)]. \quad (28)$$

It is straightforward to show that we have

$$C_0(\mathbf{k}_\parallel) = \left(\frac{\hbar\omega}{(2\pi)^3 \epsilon_0 d(I_S + I_L + I_B)}\right)^{1/2}, \qquad (29)$$

where

$$I_S = \frac{\epsilon_s}{2\beta_s d}\left(1 + \frac{k_\parallel^2}{\beta_s^2}\right), \qquad (30)$$

$$\begin{aligned} I_L = \sum_{n=0}^{N-1} \frac{\epsilon_b}{2\beta d |B_s|^2}&\left[|A_n|^2\left(1 + \frac{k_\parallel^2}{\beta^2}\right)(1 - e^{-2\beta d})\right.\\ &+ |B_n|^2\left(1 + \frac{k_\parallel^2}{\beta^2}\right)(e^{2\beta d} - 1)\\ &\left.+ \left(1 - \frac{k_\parallel^2}{\beta^2}\right)(A_n B_n^* + B_n A_n^*)\right], \end{aligned} \qquad (31)$$

$$I_B = \frac{\epsilon_b}{2\beta d}\left|\frac{A_N}{B_s}\right|^2\left(1 + \frac{k_\parallel^2}{\beta^2}\right). \qquad (32)$$

VI. DEEXCITATION RATE

A dipole emitter of dipole moment vector μ embedded within a finite charge-sheet dielectric structure is shown in Fig. 1. The interaction Hamiltonian of the dipole coupled to the electromagnetic fields of the layer structure is

$$H = \hbar\omega_0 \pi\pi^\dagger - (\pi + \pi^\dagger)\mu_{\mathbf{eg}} \cdot \hat{\mathbf{E}}(0,z) + H_{\text{field}}, \qquad (33)$$

where the dipole emitter is represented as a two-level system of states $|e\rangle$ and $|g\rangle$ with an excitation energy $\hbar\omega_0 = (E_e - E_g)$, and we define $\mu_{\mathbf{eg}} = \langle e|\mu|g\rangle$ as the (real) dipole moment vector matrix elements between states $|e\rangle$ and $|g\rangle$, π and $\pi^\dagger$ are the atomic ladder operators acting on $|e\rangle$ and $|g\rangle$, $\hat{\mathbf{E}}$ is the electric-field operator, and H_{field} is the unperturbed Hamiltonian of the electromagnetic field satisfying the electromagnetic boundary conditions at the interfaces of the structure.

For an excited dipole emitter localized at $\mathbf{r} = (0, Z_0)$, the deexcitation rate is given by Fermi's golden rule as

$$\begin{aligned} \Gamma(0,Z_0) = \frac{2\pi}{\hbar}&\int d^2\mathbf{k}_\parallel |\langle e\{0\}|\hat{\mu}\cdot\hat{\mathbf{E}}|g\{\mathbf{k}_\parallel\}\rangle|^2\\ &\times\delta(\hbar[\omega_0 - \omega(\mathbf{k}_\parallel)]), \end{aligned} \qquad (34)$$
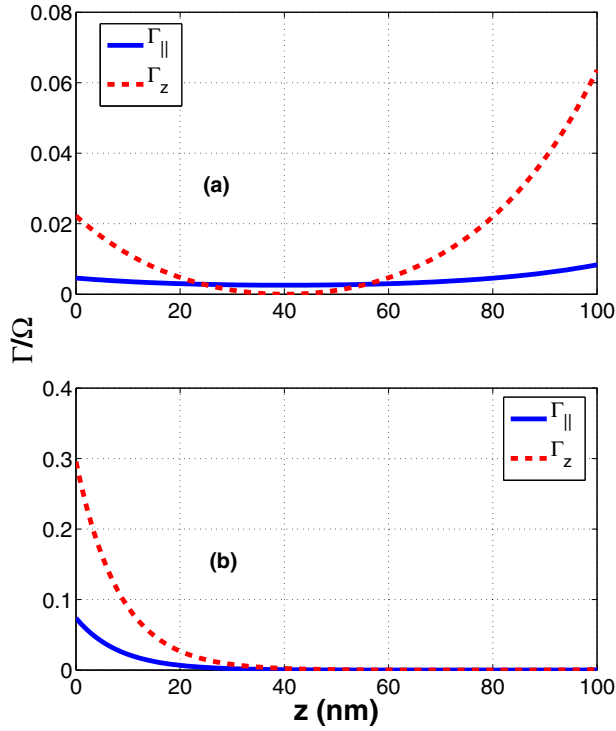
FIG. 8. (Color online) The deexcitation rates $\Gamma_\parallel$ and Γ_z in units of Ω as functions of the dipole position for normalized wave numbers for $N = 5$ and $r_s = 0.9$ and (a) $k_\parallel d = 2$, (b) $k_\parallel d = 6$, and $\Omega = 3.847 \times 10^{12}$ s^{-1}.

where the dipole moment operator $\hat{\mu}$ is defined here as $\hat{\mu} = \mu_{eg}(\pi + \pi^\dagger)$. The eigenstate $|\{0\}\rangle$ defines the corresponding vacuum state, and $|\{\mathbf{k}_\parallel\}\rangle$ corresponds to the state of wave-vector components $\mathbf{k}_\parallel$. The calculation of Γ is carried out by converting the $\mathbf{k}_\parallel$ integral to an integral over ω in order to satisfy $\omega(k_\parallel) = \omega_0$. This procedure yields the deexcitation rate as follows:

$$\Gamma(0, Z_0) = \Gamma_\parallel + \Gamma_z$$

$$= \left(\frac{2\pi \mu_{eg}}{\hbar}\right)^2 \frac{k_\parallel}{v_g} |C_0|^2 \left(\frac{\langle \mu_\parallel \rangle^2}{\mu_{eg}^2} |F|^2 + \frac{\langle \mu_z \rangle^2}{\mu_{eg}^2} |G|^2\right),$$

(35)

where $\langle \mu_\parallel \rangle = \langle \mu_{\mathbf{eg}} \cdot \hat{\mathbf{r}}_\parallel \rangle$ and $\langle \mu_z \rangle = \langle \mu_{\mathbf{eg}} \cdot \hat{\mathbf{z}} \rangle$ are dipole vector components parallel and normal to the interfaces, respectively, and μ_{eg} is defined by $\mu_{eg}^2 = \mu_\parallel^2 + \mu_z^2$. $\Gamma_\parallel$ and Γ_z are the rates parallel and normal to the interfaces. v_g is the group velocity at $k_\parallel$ given by

$$v_g = \left(\frac{\partial \omega}{\partial k_\parallel}\right)_{k_\parallel}.$$

(36)

Figure 8 displays the deexcitation rate for an emitter located at various positions in the first layer from 0 to 100 nm. Figures 8(a) and 8(b) correspond to the same parameters of the finite charge-sheet system as in Fig. 7, with normalized wave numbers of $k_\parallel d = 2$ and 6, which correspond to $\omega_0/\Omega = 1.13$ and 1.78, respectively. In Fig. 8(a), it can be seen that $\Gamma_{\parallel,z}$ increases when the emitter position is close to the interfaces and decreases towards the middle of the layer. This can

be compared to Fig. 7(a), where the intensity in the first layer correlates with the variation of the deexcitation rate. In Fig. 8(b), a higher value of $\Gamma_{\parallel,z}$ for $k_\parallel d = 6$ occurs at the dipole position near the first interface, which also corresponds to the intensity profile shown in Fig. 7(c).

Figure 9 displays Γ_z as a function of the normalized dipole transition frequency for an emitter located at $Z_0 = 0.1d$ for the cases of $r_s = 1, 0.9, 0.5$, and 2. For the case $r_s = 1$, when the bulk modes exist, Γ_z has a lower value and can be found in the full range of the normalized frequency. For the cases $r_s = 0.9, 0.5$, and 2, Γ_z is enhanced via the surface modes. A similar behavior is displayed by $\Gamma_\parallel$, but the details will not be presented here. It is clear that the surface of the structure greatly affects the deexcitation rate, which suggests that the rate can be tuned by controlling the ratio r_s.

The variations of Γ_z with the number of finite layers $N = 5, 10$, and 15 are presented in Fig. 10. It is seen that the deexcitation rate can also be controlled by a suitable choice of the number of layers N. As N increases, one can see the width of the Γ_z spectrum as well as its peak are progressively diminished, and we have checked that a similar behavior is shown by $\Gamma_\parallel$. Thus the finite charge-sheet structure with the

FIG. 9. (Color online) The deexcitation Γ_z as a function of dipole transition frequency for a dipole emitter located at $Z_0 = 0.1d$ for several permittivity ratios $r_s = 1, 0.9, 0.5$.
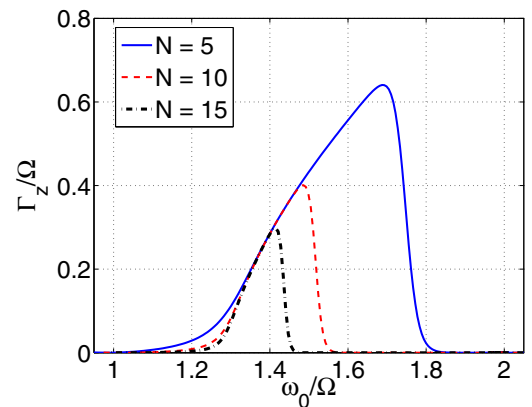
FIG. 10. (Color online) The deexcitation Γ_z spectrum for a dipole emitter located at $Z_0 = 0.1d$, $r_s = 0.9$ for several N layers: $N = 5$, 10, and 15.

surface layer $r_s \neq 1$ can effectively modify the deexcitation rate.

VII. CONCLUSIONS

The primary aim of this paper is twofold. First, we have aimed to highlight the flexibility of a system of finite ordered truncated layered structures formed of charge sheets separated by dielectric layers and sandwiched between thicker dielectric slabs in allowing the tailoring of the system for specific desirable outcomes to be achieved. Second, we were able to investigate in detail the deexcitation process and its rate for excited dipole emitters localized within the structure. The tailoring is controlled by a number of readily adjustable parameters of the system, most notably the dielectric ratio, the number of layers, the areal electron density, and the layer separation. The analytical technique for the evaluation of the layer fields in terms of transfer-matrix methods is seen to be both powerful and rather general. Significantly,

it is applicable to any number of layers. Much information can be readily extracted from the formalism, and we have seen how the frequency spectrum varies with parameters and how the field components are distributed within the structure. We have also verified that the formalism reproduces known results for single and double layers and for a finite number of layers. The study of the deexcitation process requiring properly quantized modes which satisfy the electromagnetic boundary conditions at every interface has not, as far as we know, been articulated previously for finite layer structures. Dipole emitters in the form of quantum dots, atoms, or molecules localized within the structure and regarded as two-level systems can be used as quantum bits, displaying entanglement between emitters that would be a function of the system parameters as well as the location of the emitters within the structure. Pair correlations and dipole-dipole interactions within such a structure are further applications we are currently investigating, and the results will be reported in due course.

[1] P. S. J. Russell, S. Tredwell, and P. J. Roberts, Opt. Commun. **160**, 66 (1999).

[2] I. Alvarado-Rodriguez, P. Halevi, and A. S. Sánchez, Phys. Rev. E **63**, 056613 (2001).

[3] Z. Wang, T. Zhai, J. Lin, and D. Liu, J. Opt. Soc. Am. B **24**, 2416 (2007).

[4] A. S. Sanchez and P. Halevi, Phys. Rev. E **72**, 056609 (2005).

[5] A. Kamli, M. Babiker, A. Al-Hajry, and N. Enfati, Phys. Rev. A **55**, 1454 (1997).

[6] M. Fujita, S. Takahashi, Y. Tanaka, T. Asano, and S. Noda, Science **308**, 1296 (2005).

[7] D. N. Chigrin, A. V. Lavrinenko, D. A. Yarotsky, and S. V. Gaponenko, J. Lightwave Technol. **17**, 2018 (1999).

[8] Y. Liu, R. F. Willis, K. V. Emtsev, and Th. Seyller, Phys. Rev. B **78**, 201403(R) (2008).

[9] M. G. Cottam and D. R. Tilley, *Introduction to Surface and Superlattice Excitations* (Institute of Physics, Bristol, 2005).

[10] V. Ryzhii, I. Khmyrova, M. Ryzhii, A. Satou, T. Otsuji, V. Mitin, and M. S. Shur, Int. J. High Speed Electron. Syst. **17**, 521 (2007).

[11] B. L. Johnson and R. E. Camley, Phys. Rev. B **43**, 6554 (1991).

[12] M. Liscidini, D. Gerace, D. Sanvitto, and D. Bajoni, Appl. Phys. Lett. **98**, 121118 (2011).

[13] G. F. Giuliani and J. J. Quinn, Phys. Rev. Lett. **51**, 919 (1983).

[14] E. L. Albuquerque and M. G. Cottam, Phys. Rep. **233**, 67 (1993).

[15] N. C. Constantinou and M. G. Cottam, J. Phys. C **19**, 739 (1986).

[16] G.-L. Chen, X.-F. Peng, K.-Q. Chen, and Y. Zhang, Phys. E (Amsterdam, Neth.) **41**, 1347 (2009).

[17] C. R. Bennett, M. Babiker, and J. B. Kirk, J. Mod. Opt. **49**, 269 (2002).